metals

MDPI

Article

Effect of Finish Rolling Temperature on the Microstructure and Tensile Properties of Nb–Ti Microalloyed X90 Pipeline Steel

Bin Guo [1,2], Lei Fan [1,3], Qian Wang [1,3], Zhibin Fu [1,3], Qingfeng Wang [1,3,*] and Fucheng Zhang [1,3]

1 Laboratory of Metastable Materials Science and Technology, Yanshan University, Qinhuangdao 066004, China; guobinwg@126.com (B.G.); lwc84268092wjx@163.com (L.F.); wq986086441@139.com (Q.W.); fzbknc@163.com (Z.F.); zfc@ysu.edu.cn (F.Z.)

2 Research and Development Center of WISCO, Wuhan 430080, China

3 National Engineering Research Center for Equipment and Technology of Cold Strip Rolling, Yanshan University, Qinhuangdao 066004, China

* Correspondence: wqf67@ysu.edu.cn; Tel.: +86-335-807-4631

Academic Editor: Hugo F. Lopez

Received: 12 October 2016; Accepted: 9 December 2016; Published: 20 December 2016

Abstract: The relationship between microstructure and tensile properties of an Nb–Ti microalloyed X90 pipeline steel was studied as a function of finish rolling temperature using a Gleeble 3500 simulator, an optical and scanning electron microscope, electron back scattered diffraction (EBSD), a transmission electron microscope (TEM) and X-ray diffraction. The results indicate that the microstructure is primarily composed of non-equiaxed ferrite with martensite/austenite (M/A) constituent dispersed at grain boundaries for the specimens with different finish rolling temperatures. With a decrease in the finish rolling temperature, the yield strength increases, following a significant increase in the grain refinement strengthening contribution and dislocation strengthening contribution, although the precipitation strengthening contribution decreases. The increasing yield ratio (YR) shows that the strain hardening capacity declines as a result of the microstructure evolution when decreasing the finish rolling temperature.

Keywords: X90 pipeline steel; tensile properties; grain refinement strengthening; dislocation strengthening contribution; precipitation strengthening; strain hardening capacity

1. Introduction

High-grade pipeline steels have been developed for many years to meet the requirements of the high-pressure transportation of crude oil and nature gas [1]. With the further application of pipeline steels in long-distance transportation and harsh environment, excellent toughness, weldability and deformability become more and more important, in addition to the high strength, to guarantee the safety [2–4]. Appropriate design of the microstructure is essential to achieve these targeted mechanical properties, which can be obtained by optimizing the chemical composition and the Thermo-Mechanical Control Processing (TMCP) schedule. The reheating temperature, rolling conditions (temperature and reduction), cooling rate and cooling interrupt temperature constitute the main adjustable TMCP parameters.

Much research has been executed to investigate the effects of rolling conditions on the microstructure evolution and resultant mechanical properties of high-grade microalloyed pipeline steels. The favorable microstructure with the optimum mechanical properties has been considered to be acicular ferrite (AF) for high-grade pipeline steels [5–9]. The AF could heterogeneously nucleate on particular inclusions or precipitates [10–13] and grow into intersecting ferrite plates. However, a kind of ferrite that could nucleate in the dislocation substructure of TMCP-processed steel during accelerated

continuous cooling, according to [14,15], and grow into the irregular plates, is also defined as acicular ferrite (AF). Furthermore, considering the diverse morphologies of this AF, some investigators [16–18] have proposed that the microstructure of AF is consisting of quasi-polygonal ferrite (QF), granular bainitic ferrite (GF) and even a little bainite ferrite (BF) with dispersed islands of martensite/austenite (M/A) in the matrix. The works by Kang et al. [19] and Sung et al. [20] indicated that with the decreasing finish rolling temperature, both strength and toughness were significantly improved on account of the grain refinement. The studies by Olalla et al. [21] and Kim et al. [22] further revealed that despite the decreasing precipitation strengthening contribution, the yield strength increased when the finish rolling temperature was lowered from the austenite recrystallization region to non-recrystallization region, due to the enhanced grain boundary strengthening. On the contrary, Kostryzhev et al. [23] reported that with a decrease in the austenite deformation temperature, the yield strength decreased, following a decrease in precipitation hardening, although the grain refinement contribution increased.

The study of this paper aims at investigating the relationship between the microstructure and the tensile properties of a Nb–Ti microalloyed X90 pipeline steel with a varying finish rolling temperature in the austenite non-recrystallization region. The microstructures were characterized by optical microscopy (OM), scanning electron microscopy (SEM), electron back scattering diffraction (EBSD) and transmission electron microscopy (TEM), to better understand the microstructure evolution during the simulated TMCP and clarify the microstructure units in control of the tensile properties of X90 pipeline steel.

2. Experimental Material and Procedures

The steel used in this work was a commercial X90 pipeline steel. Its chemical composition is listed in Table 1.

Table 1. Chemical compositions of the test steel (wt %).

C	Si	Mn	P	S	Mo + Ni + Cu	Nb + Ti + V
0.06	0.30	1.90	0.005	0.002	≤0.98	≤0.19

The round bar specimens with a length of 75 mm and diameter 15 mm for compressive deformation were cut from the steel pipe with the diameter × thickness of 1219 × 16.3 mm. The simulated TMCP was conducted in a Gleeble 3500 system, the schedules of which were given in Figure 1. Once reheated at 1180 °C for 10 min, all deformation schedules are applied: a simulated "roughing" step is performed at a temperature of 1080 °C with a compressive stain of 35% in the γ recrystallization region and an additional "finishing" step is performed at the temperature ranging from 850 to 790 °C, using a compressive stain of 30%. Accelerated Cooling (ACC) started at 780 °C with a 15 °C/s cooling rate, then was interrupted at 200 °C and followed by the simulated air cooling. Expansion curves (Figure 2) were also simultaneously measured during accelerated cooling, indicating that for the samples with a varying final rolling temperature from 850 to 790 °C, the transformation of $\gamma \rightarrow \alpha$ started at 530–586 °C, and all the deformations took place in the single austenite field.

To determine the austenite non-recrystallization temperature, T_{nr}, two-stage compression tests were performed in the Gleeble 3500 system where a compressive strain of 30% per each pass was applied to a group of samples of Φ10 × 15mm, with varying time intervals of 1–500 s between two passes, and temperature decreased from 1100 °C to 700 °C. The fraction of recrystallized grain was determined via quantitative metallography and plotted in Figure 3, as functions of deformation temperature and interval time, indicating that the T_{nr} is below 900 °C, and the finish rolling temperatures were situated in the non–recrystallization region.

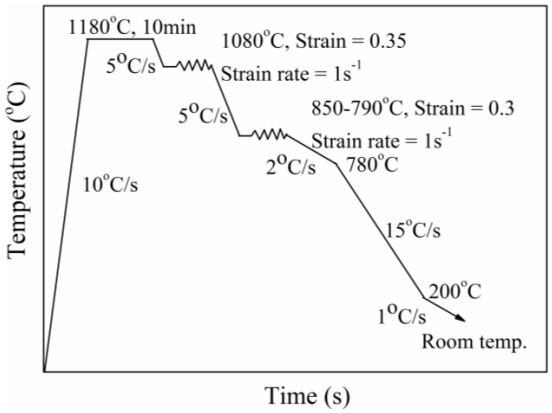

Figure 1. Graph of the simulated TMCP (thermo mechanical control process) on the Gleeble for the steel with different finish rolling temperatures.

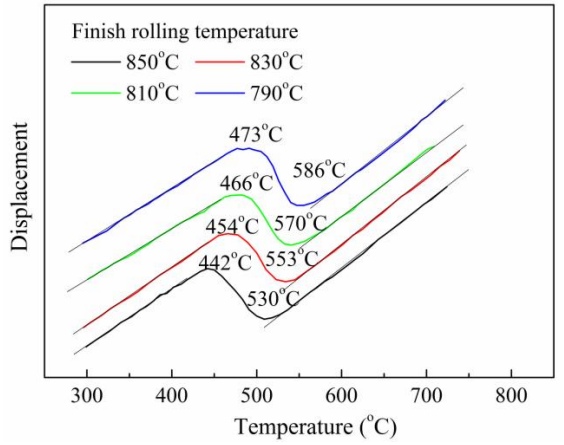

Figure 2. Expansion curves and Ar3 and Ar1 points for the samples with different finish rolling temperatures of 850–790 °C and an identical cooling rate of 15 °C/s.

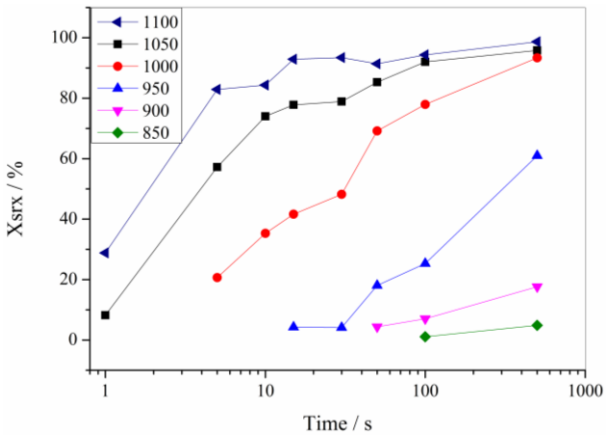

Figure 3. The fractions of recrystallized grains as functions of a varying finish rolling temperature and interval time between two passes.

After the simulation process, samples for metallographic observation were cut on the plane perpendicular to the axis of compression, and carefully prepared according to the standard method. For examination of the microstructure by Scanning Electron Microscope (SEM, Hitachi, Tokyo, Japan), a 4% nital solution was used. To observe the M/A constituent, the Lepera's reagent of 1 g sodium

metabisulfite in 100 mL distilled water mixed with 4 g of picric acid dissolved in 100 mL of alcohol was used. By this way, M/A constituent (white) and ferrite (grey phase) can be identified totally by an Optical Microscope (OM, Carl Zeiss, Oberkochen, Germany). Measurements of size and area fraction of M/A constituent were performed mainly using image analysis with the software Image-Pro Plus (Media Cybernetics, Rockville, MD, USA). For each specimen, at least 10 fields of view containing at least 1000 particles were measured at a magnification of 2000×. Thin foils for transmission electron microscopy were prepared using the twin-jet method and observed in a JEM-2010 high-resolution transmission electron microscope (TEM, JEOL, Tokyo, Japan). The carbon extraction replica technique was used to identify the morphology and size distribution of precipitates. Quantitative measurements of precipitate particles were carried out by using image analysis on a TEM image. The average size and fraction of precipitate particles were statistically measured by averaging at least 1000 particles and five fields of view containing at least 500 particles from the images of TEM, respectively. Electron back scattered diffraction (EBSD) examinations were performed on a Hitachi S-3400 Scanning Electron Microscope (SEM, Hitachi, Tokyo, Japan) equipped with a TSL EBSD system. The EBSD scan was carried out with a step size of 0.20 μm, and the EBSD effective grain size against tolerance angle ranging from 2° to 30° was calculated as the equivalent circle diameter related to the individual grain area. Moreover, the dislocation density for each sample was determined via quantitative X-ray diffraction (XRD) analysis. The XRD spectra were obtained by scanning in a Rigaku D/max-2500/PC diffractometer (Rigaku, Tokyo, Japan) over a scanning angle (2θ) range and step size of 35°–105° and 0.02°, respectively with unfiltered Cu Kα radiation. The X-ray dislocation density measuring method is based on the theory [14,24] below. Diffraction peaks are broadened by the presence of non-uniform strains that systematically shift atoms from their ideal positions, and by the finite size of coherently diffracting domains. These two effects have a different dependence on the value of θ. The non-uniform strain effect can therefore be separated, since the slope of a plot of $\beta_{hkl}\cos\{\theta_{hkl}\}$ versus $4\sin\{\theta_{hkl}\}$ is equal to a measure of the non-uniform strain ε. The parameter β is the measured peak broadening.

The micro–tensile test [25–27] specimens were wire–cut according to Figure 4 from the TMCP treated samples and tensile tested on an Inspekt Table tensile testing machine at room temperature with a cross–head speed of 0.25 mm·min^{-1}. For each simulated process, three tensile samples were tested, and the yield strength was determined by the 0.2% offset flow stress.

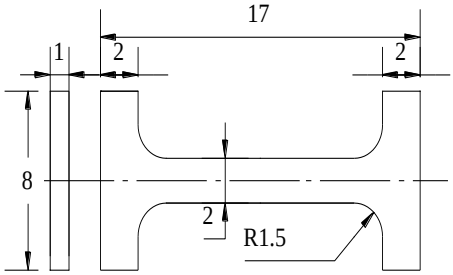

Figure 4. Wire-cut tensile specimens (in mm) from the center of the bar specimens along the transversal direction.

3. Experiment Results

3.1. Tensile Properties

The tensile properties of specimens varied with the finish rolling temperature, and are shown in Figure 5. It is indicated that the yield strength and yield ratio (YR) all increase with the decreasing finish rolling temperature, whereas the tensile strength keeps steady. The YR, which equals to the ratio of yield strength and tensile strength, is a subordinate criterion for expression of strain hardening. A lower YR represents a better strain hardening capacity.

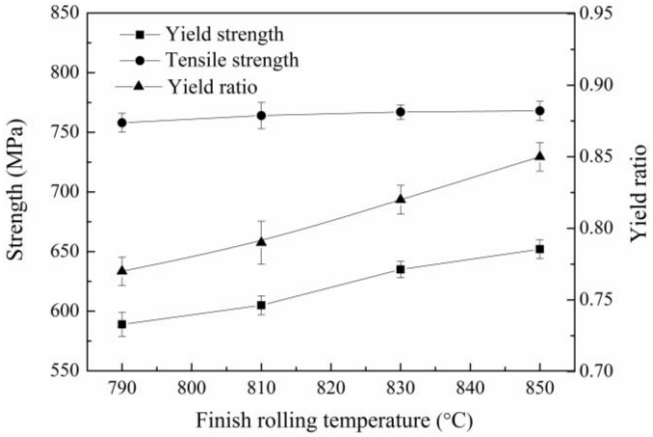

Figure 5. Results of the tensile tests, as a function of the finish rolling temperature.

3.2. Microstructure

The typical SEM micrographs of specimens as a function of the finish rolling temperature are shown in Figure 6. It is confirmed that the transformed microstructures all consist of quasi-polygonal ferrite (QF) and granular bainitic ferrite (GF) with dispersed islands of secondary phases (mainly M/A constituent) in the ferrite matrix. Based on the researches by Xiao et al. [16–18], this complicated intermediate transformation microstructure is defined as acicular ferrite (AF). The corresponding microstructure phases have been marked in the SEM micrographs of this study (Figure 6).

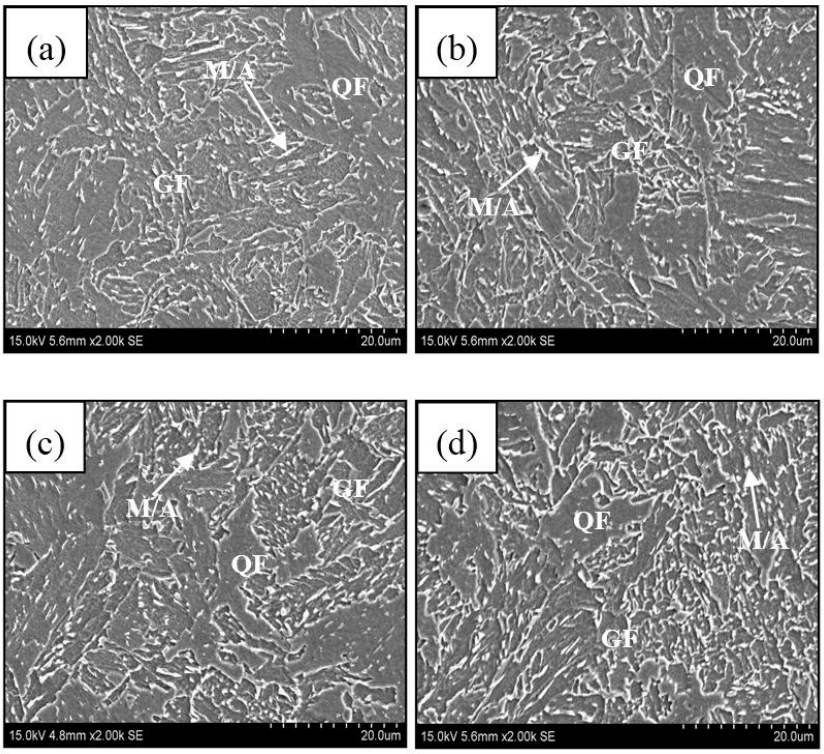

Figure 6. The SEM micrographs for the specimens with different finish rolling temperatures: (**a**) 850 °C; (**b**) 830 °C; (**c**) 810 °C and (**d**) 790 °C. QF—quasi polygonal ferrite, GF—granular bainitic ferrite and M/A—martensite/austenite.

The typical bright field TEM micrographs of specimens as a function of the finish rolling temperature are presented in Figure 7. In general, the microstructure is predominantly composed of

non-equiaxed ferrite grains with martensite/austenite (M/A) islands at grain boundaries based on TEM observations. It is revealed that both ferrite grains (white/grey) and M/A islands (black) are significantly refined when decreasing the finish rolling temperature.

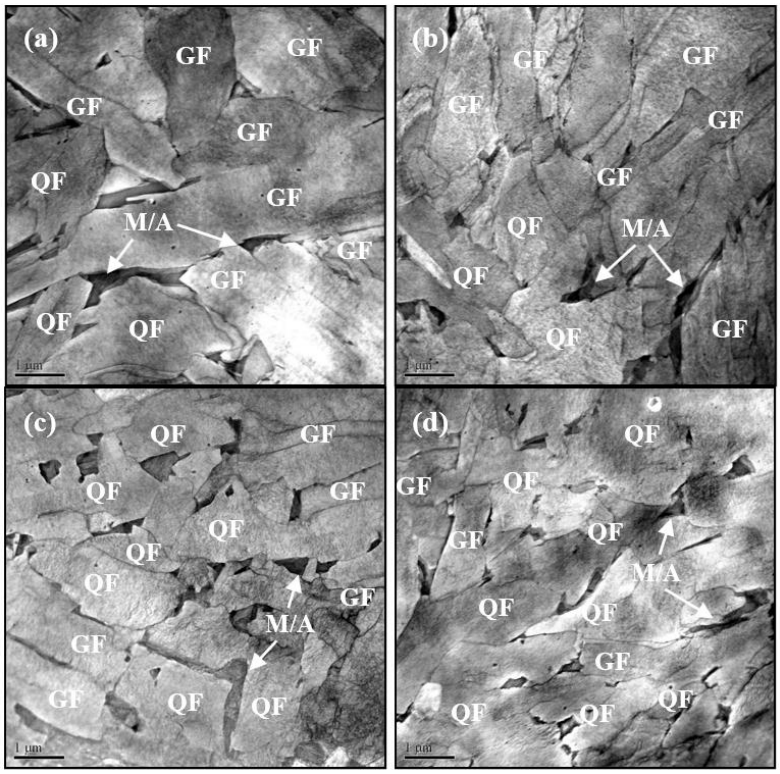

Figure 7. The TEM images of the typical microstructure morphology in the specimens with different finish rolling temperatures: (**a**) 850 °C; (**b**) 830 °C; (**c**) 810 °C and (**d**) 790 °C.

Figure 8 shows the morphology variation of M/A constituent with the finish rolling temperature. It can be seen that the coarse M/A constituent exists primarily at the grain boundaries of prior austenite and part of ferrite, with the finish rolling temperature of 850 °C and 830 °C (Figure 8a,b). When the finish rolling temperature is 810 °C, M/A constituent disperses at the ferrite boundaries and its size becomes smaller (Figure 8c). When the finish rolling temperature decreases to 790 °C, M/A constituent becomes even smaller and distributes more dispersedly with the refined ferrite grain (Figure 8d). As shown in Table 2, the amount of M/A constituent increases with the decreasing finish rolling temperature, while their mean equivalent diameter (MED) decreases.

Table 2. Results of the microstructural quantification.

Finish Rolling Temperature (°C)	M/A Constituent (%)	M/A Constituent MED (μm)	Low Angle Boundaries ($2° \leq \theta < 15°$)	
			Mean Misorientation (°)	Fraction
850	4.5 ± 0.3	1.7 ± 0.2	6.2 ± 0.2	0.40 ± 0.02
830	5.4 ± 0.4	1.5 ± 0.3	6.2 ± 0.1	0.41 ± 0.01
810	6.3 ± 0.3	1.2 ± 0.2	6.1 ± 0.2	0.43 ± 0.01
790	7.4 ± 0.2	0.8 ± 0.1	6.1 ± 0.1	0.44 ± 0.02

M/A—martensite/austenite and MED—mean equivalent diameter.

The EBSD technique has been applied for the purpose of characterizing and quantifying the microstructure. The misorientation angle figures of specimens with different finish rolling temperatures are shown in Figure 9. The EBSD effective grain size for the ferrite matrix obtained by different finish

rolling temperature has been plotted in Figure 10, as a function of the misorientation angle. It seems clear that the mean equivalent diameter (MED) of the ferrite matrix increases monotonically with the misorientation angle and the finish rolling temperature.

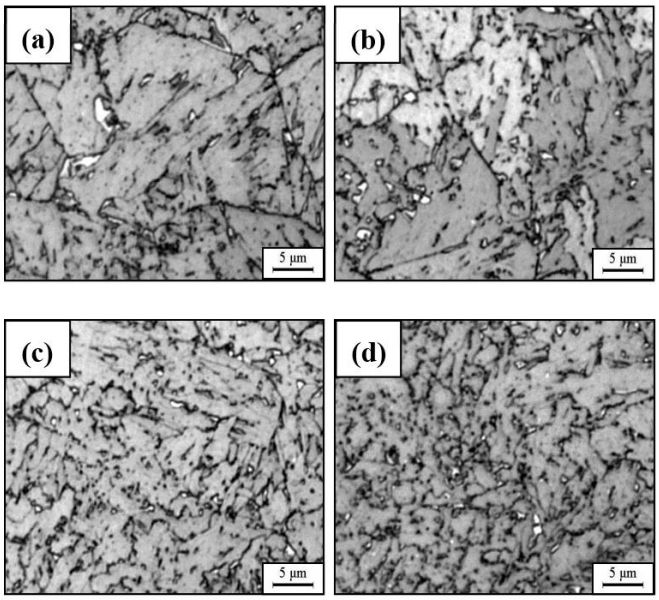

Figure 8. The M/A constituent observations at different finish rolling temperatures etched by the Lepera's reagent: (**a**) 850 °C; (**b**) 830 °C; (**c**) 810 °C and (**d**) 790 °C. Ferrite matrix is grey and M/A constituent is white. M/A—martensite/austenite.

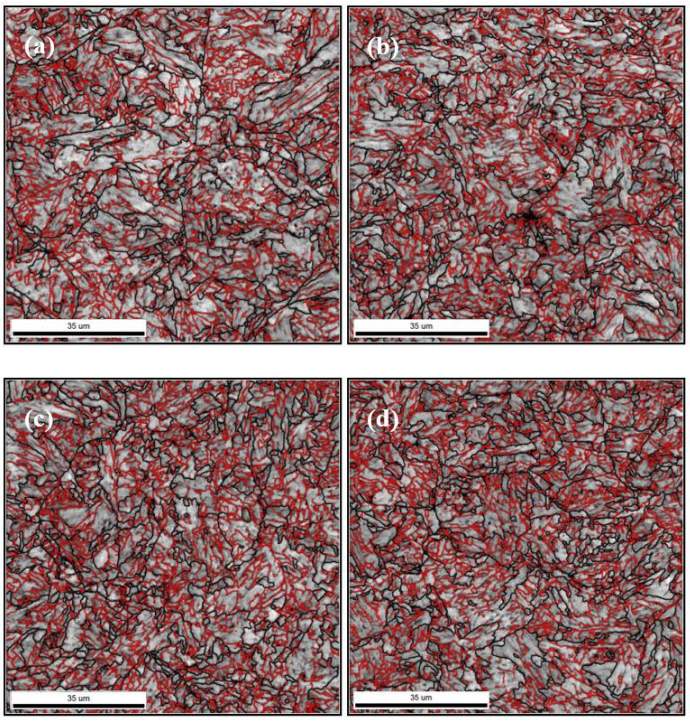

Figure 9. The EBSD (electron back-scattered diffraction) misorientation angle figures of the specimens with different finish rolling temperatures: (**a**) 850 °C; (**b**) 830 °C; (**c**) 810 °C and (**d**) 790 °C. The red line and the black line represent the misorientation angle in the range 2°–15° and greater than 15°, respectively.

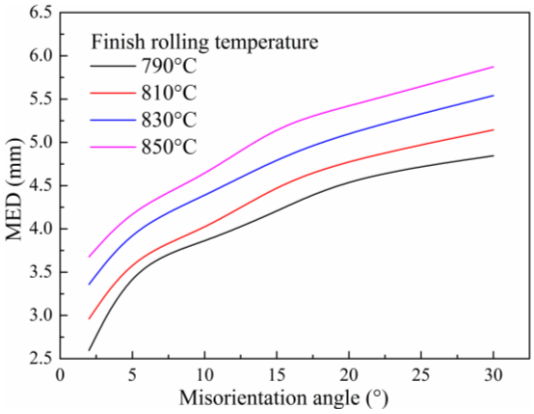

Figure 10. The EBSD mean effective size of ferrite matrix, as a function of the misorientation angle and finish rolling temperature. MED—mean equivalent diameter.

3.3. Precipitation

Figure 11 shows the bright field TEM micrographs and EDS analysis of the representative precipitates observed in the specimens with different finish rolling temperatures. The observed precipitates can be classified into two different size ranges: 10–30 nm (fine precipitates) and 30–100 nm (coarse precipitates), shown in Table 3. The smallest size range (10–30 nm) precipitates are niobium-rich carbides, while 30–100 nm cuboidal, spherical and irregular precipitates are titanium-rich and niobium-contained (Ti, Nb)C. Moreover, it can be seen that there are quite a lot of fine precipitates present in the ferrite matrix when the finish rolling temperature is 850 °C (Figure 11a), while the amount decreases a little at a finish rolling temperature of 830 °C (Figure 11b). When the finish rolling temperature is 810 °C, plenty of coarse precipitates are present in the ferrite matrix (Figure 11c). When the finish rolling temperature lowers to 790 °C, the amount of coarse precipitates becomes even larger (Figure 11d).

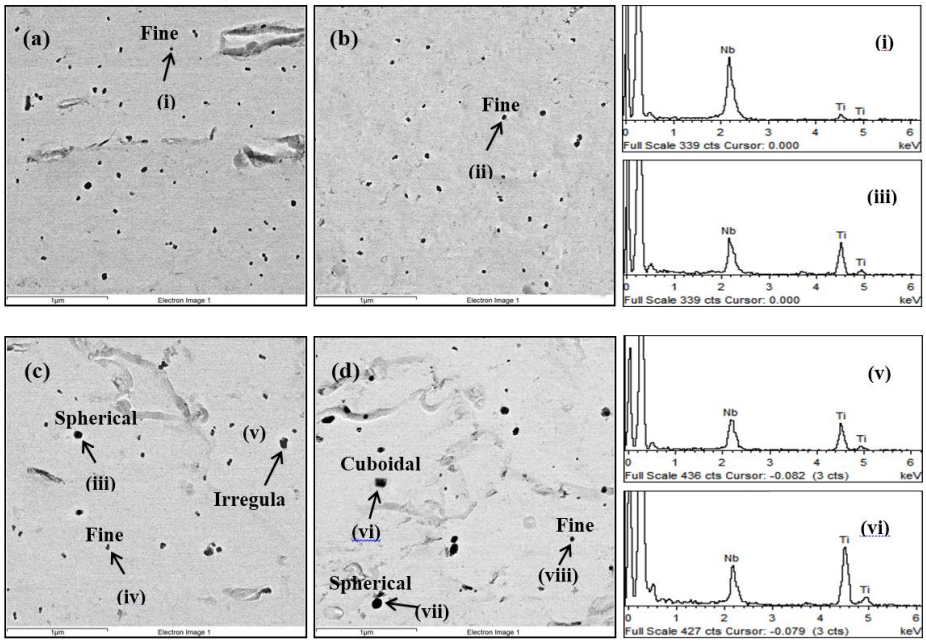

Figure 11. The TEM micrographs of the representative precipitates obtained from the specimens with different finish rolling temperatures: (**a**) 850 °C; (**b**) 830 °C; (**c**) 810 °C and (**d**) 790 °C.

Table 3. Classification of different precipitates in the test microalloyed steel.

Precipitate	Morphology	Size Range (nm)
Ti-rich (Ti, Nb)C	Spherical/Irregular Cuboidal	30–100
Nb-rich (Nb, Ti)C	Spherical	10–30

Quantification analyses of the precipitates are shown in Figure 12 and Table 4. It is revealed that the amount of the fine precipitates (10–30 nm) decreases (Figure 12), while the average size of precipitate particles increases when decreasing the finish rolling temperature (Table 4).

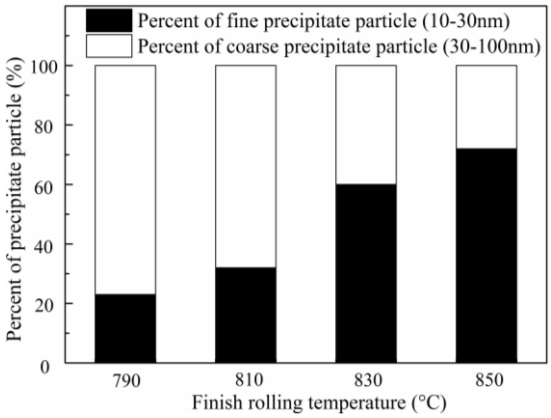

Figure 12. Percent distribution of precipitate particles of different size in the specimens varied with finish rolling temperature.

Table 4. Average precipitate size and precipitation volume fraction of the specimens varied with finish rolling temperature.

Finish Rolling Temperature (°C)	x (nm)	Volume Fraction f
850	29.3 ± 0.1	$10.8 \pm 0.2 \times 10^{-4}$
830	33.6 ± 0.2	$9.4 \pm 0.1 \times 10^{-4}$
810	48.2 ± 0.2	$8.1 \pm 0.3 \times 10^{-4}$
790	50.3 ± 0.1	$7.6 \pm 0.1 \times 10^{-4}$

x—average precipitate size, f—volume fraction.

3.4. Dislocations

Figure 13 shows the XRD patterns corresponding to samples with different finish rolling temperatures, and the dislocation densities are summarized in Table 5. As the table shows, the density of dislocations, ρ, increased with the decreasing finish rolling temperature.

Table 5. The density of dislocations of samples varied with a finish rolling temperature from 850 °C to 790 °C.

Finish Rolling Temperature (°C)	$\rho/\times 10^{14}$ m^{-2}
850	5.2 ± 0.05
830	5.9 ± 0.04
810	6.7 ± 0.07
790	7.2 ± 0.07

Note: ρ-The average dislocation density.

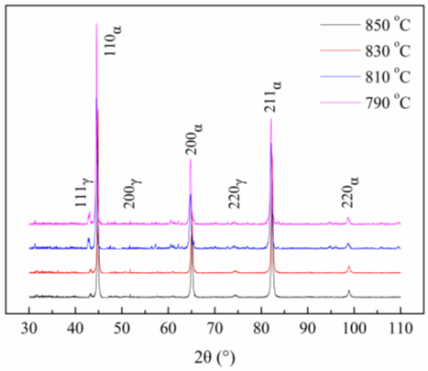

Figure 13. XRD (X-ray diffraction) spectra of samples varied with a finish rolling temperature from 850 °C to 790 °C.

4. Discussion

4.1. Effect of Finish Rolling Temperature on Microstructure Evolution

The microstructure evolution can be explained as follows. The rolling in the austenite recrystallization region brings about a continuous recrystallization of austenite grains during the rolling process and this can remarkably refine the austenite grain size [28]. Subsequently, high densities of substructure and dislocation (deformation bands) are generated in the austenite when the rolling is conducted in the non-recrystallized austenite region [29]. During the following continuous cooling process, the deformed austenite transforms into ferrite continuously, and the retained austenite is further carbon-enriched and fully stabilized until the transformation becomes thermodynamically impossible [30]. Finally, part of the carbon-enriched retained austenite could transform to martensite and the retained austenite would coexist with the martensite, making the so-called M/A constituent [31].

It is universally acknowledged that the rolling temperature plays an important role in the grain refinement and precipitation hardening by affecting prior austenite grain structure, precipitation of coarse carbides (strain induced precipitation) and dislocation substructure [22]. Because the austenite grain boundaries and deformation bands can act as the nucleation sites for austenite/ferrite phase transformation, grain refinement is enhanced with the increase of austenite grain boundary and dislocation density [32,33]. With the decreasing finish rolling temperature in the non-recrystallized austenite region, more and more deformation dislocations would be accumulated, therefore significant grain refinement has been achieved (Figure 8).

On the other hand, there occur two groups of precipitates, i.e., fine and coarse ones, in the final matrix. The coarse precipitates are made up of the Ti-rich particles, probably survived from reheating due to their high thermodynamic stability; and the Nb-rich ones, primarily coming from the strain induced precipitation in the austenite non-recrystallization zone. The well-developed dislocation structure inside the austenite grain promotes the precipitation kinetics [34]. Such strain induced precipitates will grow during the remaining process, and consequently become coarse precipitates (>30 nm). Meanwhile, the precipitation of fine articles with 10–30 nm might mainly take place during controlled cooling. Due to the precipitation of coarse carbides since the rolling process, which consumes carbide formers—Nb, Ti and C—fine precipitates (10–30 nm) are significantly reduced during the subsequent continuous cooling process. It is revealed that the amount of coarse precipitates increases with the decreasing finish rolling temperature, while the amount of fine precipitates reduces accordingly (Figures 9 and 10), leading to the decreasing average precipitate size. This is consistent with the observations made by Olalla et al. [21] and Kostryzhev et al. [23].

Moreover, the M/A constituent increases in amount, and decreases in size, as well as distributing more dispersedly while decreasing the finish rolling temperature (Figures 7 and 8 and Table 2).

According to previous work [35], a sufficient deformation strain of Fe–0.43C–3Mn–2.12Si (wt %) steel can lead to a mechanical stabilization of austenite to some degree, and accordingly lower the onset temperature of bainitic transformation. However, for the present experimental steel, the decreasing finish rolling temperature corresponds to an elevated onset temperature (Ar_3) of $\gamma \rightarrow$ QF + GF (Figure 2), indicating that the initial stability of deformed austenite is reduced, possibly due to the increased dislocation substructure acting as the nucleation site for QF and GF. Nevertheless, the continuous cooling phase transformation of $\gamma \rightarrow \alpha + \gamma'$ (metastable austenite) is accompanied by the partitioning of carbon atoms from α to γ' through the dislocation related pipe diffusion and bulk diffusion [22,34], resulting in C-rich γ' with correspondingly elevated stability. Therefore, it could be proposed that due to the decreasing finish rolling temperature, the increased dislocation structure would enhance the stability of austenite during the subsequent continuous cooling transformation, and accordingly result in an increasing amount of M/A constituent. Simultaneously, locations for M/A constituent at the ferrite boundaries become more scattered and their size decreases because of grain refinement.

4.2. Effect of Finish Rolling Temperature on Tensile Properties

The yield strength of Nb–Ti microalloyed pipeline steel can be described by a linear sum of the individual strengthening contributions; i.e.,

$$\sigma_y = \sigma_0 + \sigma_s + \sigma_d + \sigma_{dis} + \sigma_{ph} + \sigma_{M\text{-}A} \quad (1)$$

where σ_0: lattice friction stress; σ_s: solid solution strengthening, owing to interstitial and substitutional atoms; σ_d: strengthening provided by the boundaries of the GBF (granular bainitic ferrite) and AF effective grain; σ_{dis}: dislocation strengthening of the GBF and AF; σ_{ph}: carbonitride precipitation strengthening; $\sigma_{M\text{-}A}$: strengthening owing to the hard M/A constituent. The YS (yield strength) is affected by each of these strengthening factors in varying degrees. For the present study, the values of these strengthening factors are calculated to better understand the strengthening mechanism of the experimental steel.

The calculation of grain boundary strengthening is by the Hall–Petch equation, based on the EBSD test results. According to [36], the lowest threshold angle that provides a consistent crystallite size quantification from EBSD scans has been estimated experimentally at 2°, irrespective of the type of microstructure. Moreover, the contribution of very low angle boundaries with a misorientation $\theta < 2°$ to strength can be regarded as part of the total dislocation strengthening, while the rest of boundaries with a misorientation $\theta \geq 2°$ contribute to the boundary strengthening. In this attempt, the EBSD effective size corresponds to the boundaries with a misorientation $2° \leq \theta \leq 30°$. In detail, high angle boundaries ($\theta \geq 15°$) are relevant to the bainitic packets/sheaves, according to [36], while low angle boundaries ($2° \leq \theta < 15°$) are related to the ferrite sub-units within the bainitic packets/sheaves. High angle boundaries ($\theta \geq 15°$) are expected to contribute with an orientation independent Hall–Petch coefficient, k_{HP}, while the strength of low angle boundaries ($2° \leq \theta < 15°$) depends on the misorientation [37]:

$$k_{HP}(\theta) = k\alpha M\mu\sqrt{b\theta} \quad (2)$$

in which k is a proportionality constant of the order of 1, while α, M, μ and b represent a constant, the Taylor factor, the shear modulus and the Burgers vector, respectively [37].

The following expression has been recently deduced [36]:

$$\sigma_d = k_{HP}(MED_{2°})^{-0.5} \cong 1.05\alpha M\mu\sqrt{b}\left[\sum_{2° \leq \theta_i < 15°} f_i\sqrt{\theta_i} + \sqrt{\frac{\pi}{10}}\sum_{\theta_i \geq 15°} f_i\right](MED_{2°})^{-0.5} \quad (3)$$

where f_i and θ_i are, respectively, the relative frequency and the mean misorientation angle (rad) in the interval i (Table 2), and $MED_{2°}$ is the mean equivalent diameter of ferrite matrix effective grain

with a misorientation angle of 2°, determined by EBSD (Figure 10). In this equation, the Hall–Petch coefficient can directly be obtained from the EBSD scans, irrespective of the type of microstructure.

For the specimens varied with the finish rolling temperature, the computed σ_d values from Equation (3) with $\alpha = 0.3$, $M = 3$, $\mu = 8 \times 10^4$ MPa and $b = 2.5 \times 10^{-7}$ mm [36] are shown in Figure 14. It is indicated that with the decreasing finish rolling temperature, the grain boundary strengthening contribution increases significantly.

The estimation of precipitation strengthening is studied by using the Orowan–Ashby equation, as shown in Equation (4):

$$\tau_{ppt} = \frac{1.2Gb}{2.36\pi L} \ln(x/2b) \quad (4)$$

where τ_{ppt} is the shear stress, x is the average planar intersect diameter of the particles, G is the shear modulus (81.6 GPa for Fe), b is the Burger's vector (0.248 nm for Fe), and L is the average free distance between particles on the slip plane, and L is described as follows:

$$L = x(\pi/4f)^{1/2} \quad (5)$$

f is the volume fraction of the precipitates and can be evaluated by quantitative metallography [38]. Substituting Equation (5) into Equation (4) and multiplying the shear stress by a Taylor factor M (3.06 [39]) to convert the shear stress to uniaxial yield stress [40], the Orowan–Ashby equation is:

$$\sigma_{ppt} = \frac{11.3f^{1/2}}{x} \ln(x/4.96 \times 10^{-4}) \quad (6)$$

The precipitate quantification (average precipitate size and precipitation volume fraction) and precipitation strengthening value of the specimens varied with the finish rolling temperature and are shown in Table 4 and Figure 14, respectively. It can be seen that there is a less obvious precipitation strengthening decrement when decreasing the finish rolling temperature. It is indicated in Figure 14 that the precipitation strengthening contribution decreases with the decreasing finish rolling temperature.

The contribution of dislocation strengthening to the YS can be estimated from [41]:

$$\sigma_{dis} = \alpha MGb\rho^{1/2} \quad (7)$$

where α, M, G, b, and ρ are a constant (i.e., 0.15), Taylor factor (2.73 for ferrite steel), shear modulus (81.6 GPa for Fe), Burger's vector (0.248 nm for Fe), and the average dislocation density, respectively; ρ was determined experimentally from the XRD spectrum of each steel shown in Figure 13. The strengthening contribution from the dislocations of each sample is summarized in Figure 14. As the table shows, the average dislocation density of the GF and QF, which inherit the dislocations of deformed austenite during accelerated cooling transformation, increases with decreasing finish rolling temperature, thereby leading to an increase in the contribution from dislocation strengthening.

In addition to the aforementioned strengthening mechanisms, the sum of other individual strengthening contributions, $\sigma_0 + \sigma_s + \sigma_{M\text{-}A}$ is calculated using the following method:

$$\sigma_0 + \sigma_s + \sigma_{M\text{-}A} = \sigma_y - (\sigma_d + \sigma_{dis} + \sigma_{ph})$$

The result presented in Figure 13. shows that the sum of other individual strengthening contributions, $\sigma_0 + \sigma_s + \sigma_{M\text{-}A}$ changes from 56 Mpa to 71 Mpa and only accounts for a small proportion of the overall yield strength.

Excluding the sum $\sigma_0 + \sigma_s + \sigma_{M\text{-}A}$, the individual factors may be written in descending order of their strengthening contribution as, effective grain of the GF and QF, dislocations, and precipitates. On the other hand, effective grain size decreased and the dislocation density increased with the finish rolling temperature decreasing. However, the decreasing finish rolling temperature also resulted

in a decrease in the density of fine precipitates and in turn resulted in a decreased strengthening contribution. However, the effect of the former overwhelms the latter, as a result, the overall YS increases with the decreasing finish rolling temperature.

Several researches have been carried out to deal with the relationship between the yield strength and microstructure in microalloyed steels. Kim et al. [22] revealed that despite the decreasing precipitation strengthening contribution, the yield strength increased when decreasing the finish rolling temperature due to the enhanced grain boundary strengthening and dislocation strengthening. The present results are in good agreement with the previous works above on the relationship between the yield strength and different microstructure.

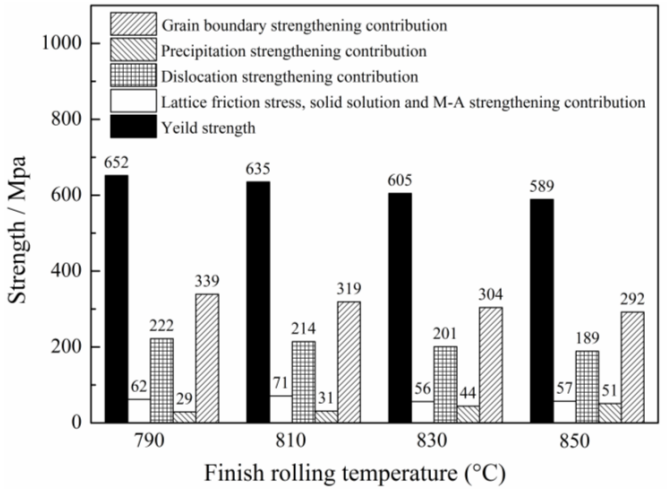

Figure 14. Results of contribution values of different kinds of strengthening mechanisms, as a function of the finish rolling temperature.

Furthermore, when decreasing the finish rolling temperature, not only the yield strength increases but also the yield ratio (YR), indicating that the yield strength increases faster than the tensile strength. The YR, which equals to the ratio of yield strength and tensile strength, is a critical subordinate criteria for the expression of strain hardening [42]. The increase of the YR suggests that the strain hardening capacity declines.

It can be seen from Figure 3 that the YR increases with the decreasing M/A constituent area fraction (Table 2) and ferrite matrix effective grain size (Figure 8) originated from the decreasing finish rolling temperature, indicating a decreasing strain hardening capacity. The increasing YR suggests that the yield strength increases much faster than the tensile strength when the finish rolling temperature decreases. This is mainly because grain refinement contributes more to the yield strength, while the tensile strength is not sensitive to grain size [25,43]. Besides, the slight decrease of hard phase (M/A constituent) fraction would also lead to the decline of strain hardening ability and the consequent increase of the YR based on the multiphase steel micromechanics models [44]. Hence, the increasing YR is the suggestion, revealing that a declining strain hardening capacity would be obtained when decreasing the finish rolling temperature.

5. Conclusions

The microstructure and the tensile properties of a Nb–Ti microalloyed X90 pipeline steel with a varying finish rolling temperature have been investigated in this work. The conclusions are as follows:

1. The microstructure is primarily composed of non–equiaxed ferrite with martensite/austenite (M/A) constituent dispersed at grain boundaries for the specimens with different finish rolling temperatures. With the finish rolling temperature decreased, ferrite grains are refined and M/A constituent becomes smaller accompanied by a decrease of amount.

2. With the decreasing finish rolling temperature, the yield strength increases, despite the declining precipitation strengthening contribution. This indicates that the increasing grain boundary strengthening contribution and the dislocation strengthening contribution overwhelm the decreasing precipitation strengthening part and are the dominating strengthening mechanism of the steel.
3. The strain hardening capacity gradually declines, indicated by the increase of the yield ratio when the finish rolling temperature decreases, which are the consequences of decrements derived from the decreasing amount of hard M-A constituent and the refined ferrite grain, respectively.

Acknowledgments: This work is financially supported by the Research and Development Center of Wuhan Iron and Steel (Group) Company of China under the Contract No. 2014Z05 and by the National Natural Science Foundation of China (Grant No. 51471142 and No. 5167010961).

Author Contributions: Qingfeng Wang and Bin Guo conceived and designed the experiments; Lei Fan performed the experiments; Fucheng Zhang and Qian Wang analyzed the data; Zhibin Fu contributed analysis tools; Qingfeng Wang and Bin Guo wrote the paper.

Conflicts of Interest: The authors declare no conflict of interest.

References

1. Zhao, M.C.; Yang, K.; Shan, Y. The effects of thermo-mechanical control process on microstructures and mechanical properties of a commercial pipeline steel. *Mater. Sci. Eng. A* **2002**, *335*, 14–20. [CrossRef]
2. Kim, Y.M.; Kim, S.K.; Lim, Y.J.; Kim, N.J. Effect of microstructure on the yield ratio and low temperature toughness of linepipe steels. *ISIJ Int.* **2002**, *42*, 1571–1577. [CrossRef]
3. Bott, I.; de Souza, L.F.G.; Teixeira, J.C.G.; Rios, P.R. High-strength steel development for pipelines: A brazilian perspective. *Metall. Mater. Trans. A* **2005**, *36A*, 443–454. [CrossRef]
4. Xu, J.; Misra, R.D.K.; Guo, B.; Jia, Z.; Zheng, L. Understanding variability in mechanical properties of hot rolled microalloyed pipeline steels: Process–structure–property relationship. *Mater. Sci. Eng. A* **2013**, *574*, 94–103. [CrossRef]
5. Smith, Y.E.; Coldren, A.P.; Cryderman, R.L. *Toward Improved Ductility and Toughness*; Climax Molybdenum Company (Japan) Ltd.: Tokyo, Japan, 1972; pp. 119–142.
6. Wang, W.; Yan, W.; Zhu, L.; Hu, P.; Shan, Y.; Yang, K. Relation among rolling parameters, microstructures and mechanical properties in an acicular ferrite pipeline steel. *Mater. Des.* **2009**, *30*, 3436–3443. [CrossRef]
7. Kong, J.; Zhen, L.; Guo, B.; Li, P.; Wang, A.; Xie, C. Influence of Mo content on microstructure and mechanical properties of high strength pipeline steel. *Mater. Des.* **2004**, *25*, 723–728.
8. Sun, J.-Q.; Dai, H.; Zhang, Y.-C. Research on mathematical model of thermal deformation resistance of X80 pipeline steel. *Mater. Des.* **2011**, *32*, 1612–1616. [CrossRef]
9. Shanmugam, S.; Misra, R.D.K.; Hartmann, J.E.; Jansto, S.G. Microstructure of high strength niobium-containing pipeline steel. *Mater. Sci. Eng. A* **2006**, *441*, 215–229. [CrossRef]
10. Babu, S.S. The mechanism of acicular ferrite in weld deposits. *Curr. Opin. Solid State Mater. Sci.* **2004**, *8*, 267–278. [CrossRef]
11. Babu, S.S.; Bhadeshia, H.K.D.H. Transition from Bainite to Acicular Ferrite in Reheated Fe-Cr-C Weld Deposits. *Mater. Sci. Technol.* **1990**, *6*, 1005–1020. [CrossRef]
12. Byun, J.S.; Shim, J.H.; Suh, J.Y.; Oh, Y.J.; Cho, Y.W.; Shim, J.D.; Lee, D.N. Inoculated acicular ferrite microstructure and mechanical properties. *Mater. Sci. Eng. A* **2001**, *319*, 326–331. [CrossRef]
13. Diaz-Fuentes, M.; Gutierrez, I. Analysis of different acicular ferrite microstructures generated in a medium-carbon molybdenum steel. *Mater. Sci. Eng. A* **2003**, *363*, 316–324. [CrossRef]
14. Yakubtsov, I.A.; Poruks, P.; Boyd, J.D. Microstructure and mechanical properties of bainitic low carbon high strength plate steels. *Mater. Sci. Eng. A* **2008**, *480*, 109–116. [CrossRef]
15. Yakubtsov, I.A.; Boyd, J.D. Bainite transformation during continuous cooling of low carbon microalloyed steel. *Mater. Sci. Technol.* **2001**, *17*, 296–301. [CrossRef]
16. Li, X.; Fan, Y.; Ma, X.; Subramanian, S.V.; Shang, C. Influence of martensite-austenite constituents formed at different intercritical temperatures on toughness. *Mater. Des.* **2014**, *67*, 457–463. [CrossRef]
17. Wang, B.X.; Liu, X.H.; Wang, G.D. Effect of deformation of austenite and cooling rates on transformation microstructures in a Mn–Cr gear steel. *Mater. Des.* **2009**, *30*, 2198–2204. [CrossRef]

18. Wang, W.; Shan, Y.; Yang, K. Study of high strength pipeline steels with different microstructures. *Mater. Sci. Eng. A* **2009**, *502*, 38–44. [CrossRef]
19. Kang, N.; Lee, Y.; Byun, S.; Kim, K.; Chuang, J.; Cho, K. Quantitative analysis of microstructural and mechanical behavior for Fe–0.1C–(V, Nb) steels as a function of the final rolling temperature. *Mater. Sci. Eng. A* **2009**, *499*, 157–161. [CrossRef]
20. Sung, H.K.; Sohn, S.S.; Shin, S.Y.; Lee, S.; Kim, N.J.; Chon, S.H.; Yoo, J.Y. Effects of finish rolling temperature on inverse fracture occurring during drop weight tear test of API X80 pipeline steels. *Mater. Sci. Eng. A* **2014**, *541*, 181–189. [CrossRef]
21. Olalla, V.C.; Bliznuk, V.; Sanchez, N.; Thibaux, P.; Kestens, L.A.I.; Petrov, R.H. Analysis of the strengthening mechanisms in pipeline steels as a function of the hot rolling parameters. *Mater. Sci. Eng. A* **2014**, *604*, 46–56. [CrossRef]
22. Kim, Y.W.; Kim, J.H.; Hong, S.G.; Lee, C.S. Effects of rolling temperature on the microstructure and mechanical properties of Ti–Mo microalloyed hot-rolled high strength steel. *Mater. Sci. Eng. A* **2014**, *605*, 244–252. [CrossRef]
23. Kostryzhev, A.G.; Al Shahrani, A.; Zhu, C.; Cairney, J.M.; Ringer, S.P.; Killmore, C.R.; Pereloma, E.V. Effect of niobium clustering and precipitation on strength of an NbTi-microalloyed ferritic steel. *Mater. Sci. Eng. A* **2014**, *607*, 226–235. [CrossRef]
24. García-Mateo, C.; Caballero, F.G.; Bhadeshia, H.K.D.H. Mechanical properties of low-temperature bainite. *Mater. Sci. Forum* **2005**, *500–501*, 495–502. [CrossRef]
25. Tang, Z.; Stumpf, W. The effect of microstructure and processing variables on the yield to ultimate tensile strength ratio in a Nb–Ti and a Nb–Ti–Mo line pipe steel. *Mater. Sci. Eng. A* **2008**, *490*, 391–402. [CrossRef]
26. Liu, H.; Lu, X.; Jin, X.; Dong, H.; Shi, J. Enhanced mechanical properties of a hot stamped advanced high-strength steel treated by quenching and partitioning process. *Scr. Mater.* **2011**, *64*, 749–752. [CrossRef]
27. Fan, L.; Wang, T.; Fu, Z.; Zhang, S.; Wang, Q. Effect of heat-treatment on-line process temperature on the microstructure and tensile properties of a low carbon Nb-microalloyed steel. *Mater. Sci. Eng. A* **2014**, *607*, 559–568. [CrossRef]
28. Han, Y.; Shi, J.; Xu, L.; Cao, W.Q.; Dong, H. Effect of hot rolling temperature on grain size and precipitation hardening in a Ti-microalloyed low-carbon martensitic steel. *Mater. Sci. Eng. A* **2012**, *553*, 192–199. [CrossRef]
29. Kim, Y.M.; Lee, H.; Kim, N.J. Transformation behavior and microstructural characteristics of acicular ferrite in linepipe steels. *Mater. Sci. Eng. A* **2008**, *478*, 361–370. [CrossRef]
30. Wang, S.C.; Yang, J.R. Effects of chemical composition, rolling and cooling conditions on the amount of martensite/austenite (M/A) constituent formation in low carbon bainitic steels. *Mater. Sci. Eng. A* **1992**, *154*, 43–49. [CrossRef]
31. Fan, L.; Zhou, D.; Wang, T.; Li, S.; Wang, Q. Tensile properties of an acicular ferrite and martensite/austenite constituent steel with varying cooling rates. *Mater. Sci. Eng. A* **2014**, *590*, 224–231. [CrossRef]
32. Calvo, J.; Jung, I.H.; Elwazri, A.M.; Bai, D.; Yue, S. Influence of the chemical composition on transformation behaviour of low carbon microalloyed steels. *Mater. Sci. Eng. A* **2009**, *520*, 90–96. [CrossRef]
33. Lanzagorta, J.L.; Jorge-Badiola, D.; Guiterrez, I. Effect of the strain reversal on austenite–ferrite phase transformation in a Nb-microalloyed steel. *Mater. Sci. Eng. A* **2010**, *527*, 934–940. [CrossRef]
34. Dutta, B.; Palmiere, E.J.; Sellars, C.M. Modelling the kinetics of strain induced precipitation in Nb microalloyed steels. *Acta Mater.* **2001**, *49*, 785–794. [CrossRef]
35. Chatterjee, S.; Wang, H.S.; Yang, J.R.; Bhadeshia, H.K.D.H. Mechanical stabilisation of austenite. *Mater. Sci. Technol.* **2006**, *22*, 641–644. [CrossRef]
36. Iza-Mendia, A.; Gutiérrez, I. Generalization of the existing relations between microstructure and yield stress from ferrite–pearlite to high strength steels. *Mater. Sci. Eng. A* **2013**, *561*, 40–51. [CrossRef]
37. Hansen, N.; Huang, X.; Winther, G. Grain orientation, deformation microstructure and flow stress. *Mater. Sci. Eng. A* **2008**, *494*, 61–67. [CrossRef]
38. Kestenbach, H. Dispersion hardening by niobium carbonitride precipitation in ferrite. *Mater. Sci. Technol.* **1997**, *13*, 731–739. [CrossRef]
39. Stoller, R.E.; Zinkle, S.J.; Nucl, J. On the relationship between uniaxial yield strength and resolved shear stress in polycrystalline materials. *J. Nucl. Mater.* **2000**, *283–287*, 349–352. [CrossRef]
40. Rosenberg, J.M.; Piehle, H.R. Calculation of the taylor factor and lattice rotations for bcc metals deforming by pencil glide. *Metall. Mater. Trans.* **1971**, *2B*, 257–259. [CrossRef]

41. Hughes, D.A. Microstructure evolution, slip patterns and flow stress. *Mater. Sci. Eng. A* **2001**, *319–321*, 46–54. [CrossRef]
42. Zare, A.; Ekrami, A. Effect of martensite volume fraction on work hardening behavior of triple phase (TP) steels. *Mater. Sci. Eng. A* **2011**, *528*, 4422–4426. [CrossRef]
43. Prasad, S.N.; Sarma, D.S. Influence of thermomechanical treatment on microstructure and mechanical properties of Nb bearing weather resistant steel. *Mater. Sci. Eng. A* **2005**, *408*, 53–63. [CrossRef]
44. Ishikawa, N.; Parks, D.M.; Kurihara, M. Micromechanism of Ductile Crack Initiation in Structural Steels Based on Void Nucleation and Growth. *ISIJ Int.* **2000**, *40*, 519–527. [CrossRef]